

Parton radiative processes and pressure isotropization in relativistic heavy ion collisions

Bin Zhang and Warner A. Wortman

*Department of Chemistry and Physics, Arkansas State University,
P.O. Box 419, State University, AR 72467-0419, U.S.A.*

Abstract

The impact of radiative processes on kinetic equilibration is studied via a radiative transport model. The $2 \leftrightarrow 3$ processes can significantly increase the level of thermalization. These processes lead to an approximate coupling constant scaling of the evolution of the pressure anisotropy qualitatively different from the case with only $2 \rightarrow 2$ partonic processes. Furthermore, thermal and Color Glass Condensate motivated initial conditions are shown to share the same asymptotic evolution when $2 \leftrightarrow 3$ processes are included. This emphasizes the unique role of radiative processes in Quark-Gluon Plasma thermalization.

Keywords: Relativistic Heavy Ion Collisions, kinetic equilibration, radiative transport

PACS: 25.75.-q, 25.75.Nq, 24.10.Lx

1. Introduction

The Quark-Gluon Plasma can be produced in central relativistic heavy ion collisions [1–4]. It leads to strong collective flow and jet quenching. Ideal hydrodynamics is very successful in describing experimental observables in the low transverse momentum region [5–8]. Transport models can also give good descriptions of global observables in these collisions [9–16]. Ideal hydrodynamics assumes local thermal equilibrium and the ideal hydrodynamic equations are valid when there is local isotropization [17]. It is interesting to study the effects of viscosity [18–24] and how the partons produced in heavy ion collisions thermalize [25–28]. The equilibration process can be studied with a microscopic transport model [29–32]. In particular, Xu

and Greiner studied the transport rates [29] and showed that radiative processes are important for parton momentum isotropization. A related topic is pressure isotropization. The Frankfurt group extended the viscous hydrodynamic equation to the third order [32] for the pressure isotropization study. They compared pressure anisotropy evolutions starting from an isotropic initial condition with both the extended viscous hydrodynamics and an elastic parton cascade with time dependent cross sections. The comparison demonstrates the importance of higher order corrections in describing highly viscous matters. In the following, we will study whether and how pressure isotropization depends on the inclusion of radiative processes. The pressure anisotropy evolutions with different initial anisotropies, energy densities, fugacities, momentum distributions, coupling constants will be compared and contrasted to demonstrate the effects of radiative processes. We will further discuss how the system loses memory of the initial pressure anisotropy to approach the common asymptotic evolution and the interplay between chemical equilibration and kinetic equilibration.

2. Pressure Isotropization and radiative transport

Relativistic heavy ion collisions produce hot and dense matter. The highest energy density is achieved in the central cell in central collisions. Kinetic equilibration in the central cell can be characterized by the pressure anisotropy parameter, i.e., the longitude pressure to the transverse pressure ratio P_L/P_T . When there is thermal equilibrium, the pressure anisotropy equals one. Any pressure anisotropy value that is not equal to one indicates non-equilibrium conditions.

We will study the early stage when longitudinal expansion dominates the central cell evolution. The initial conditions will be taken to be similar to those expected in central relativistic heavy ion collisions. Only massless gluons are included and the formation proper time is set to be 0.5 fm/c. These gluons will be distributed uniformly inside a transverse circle with a radius of 5 fm and a space-time rapidity region from -5 to +5. The initial space-time rapidity density $dN/d\eta_s = 1000$. The partonic system can start with an initial energy density $\epsilon_0 = 38.2$ GeV/fm³ or 76.4 GeV/fm³. In the local rest frame, the initial particle distribution can be isotropic or transverse. Both have exponential momentum distributions. In the isotropic case, $\epsilon_0 = 38.2$ GeV/fm³ is equivalent to an initial temperature of $T_0 = 0.5$ GeV and $\epsilon_0 = 76.4$ GeV/fm³ corresponds to an initial temperature of 1 GeV. The

transverse initial conditions are isotropic in the transverse plane with an initial temperature 50% higher than the isotropic case to have the same initial energy density.

To study the effects of radiative processes, we will compare results with only the $2 \rightarrow 2$ process that has 2 incoming gluons and 2 outgoing gluons with those including additional $2 \leftrightarrow 3$ processes. The $2 \rightarrow 2$ cross section is set to be the perturbative QCD cross section regulated by a Debye screening mass, i.e.,

$$\sigma_{22} = \frac{9\pi\alpha_s^2}{2\mu^2}. \quad (1)$$

In the above formula, α_s is the strong interaction coupling constant and μ is the Debye screening mass. The Debye screening mass is calculated dynamically via

$$\mu^2 = \frac{3\pi\alpha_s}{V} \sum_i \frac{1}{p_i}, \quad (2)$$

where V is the volume of the cell and the sum goes over all gluons in the cell.

The effect of dynamical screening can be demonstrated by comparing the collision rate with the expansion rate. In a fixed box, evolution from a pressure anisotropy different from 1 is characterized by the collision rate only. However, when the system undergoes longitudinal expansion, there is a tendency of evolving toward 0 pressure anisotropy. The initial pressure anisotropy and the expansion rate are responsible for how fast this happens. It is the competition between collision and expansion that determines whether pressure isotropization can happen. For the simple case when the system can be approximately described by a temperature T , the cross section $\sigma \propto 1/\mu^2 \propto 1/T^2$. The collision rate $R_c = n\sigma \propto T^3 \times 1/T^2 \sim T \propto 1/\tau^{1/3}$. In the above formula, n stands for the particle number density and the relation between T and the proper time τ for the Bjorken expansion is used. The volume expansion rate $R_v \propto 1/\tau$. It decreases faster than the collision rate. Therefore, even if the initial expansion rate is large and there is a large initial pressure anisotropy, resulting in a decrease of pressure anisotropy toward 0, the collision rate will eventually take over and pressure anisotropy will evolve toward 1.

The $2 \leftrightarrow 3$ radiative processes are implemented for the study of the importance of radiative processes. In particular, the $2 \rightarrow 3$ cross section is taken to be 1/2 of the $2 \rightarrow 2$ cross section. This is in line with a more elaborate study by Xu and Greiner [15]. To ensure the correct chemical

equilibrium, the detailed balance relation needs to be enforced for the $3 \rightarrow 2$ process. We will take all outgoing particles to be isotropic in the center of mass frame of the collision. This is expected to reflect the gross features of particle production in the central region. The $3 \rightarrow 2$ collision rate is related to the reaction integral I_{32} , i.e., the integral over the phase space volume (with proper summation and averaging over internal degrees of freedom) of the modulus squared of the transition matrix element M . In this case, $I_{32} = \frac{1}{2!} \frac{d^2}{(2\pi)^{3 \times 2}} |M|^2 (2\pi)^4 R_2(s^{1/2}, 0, 0)$, where $d = 16$ is the gluon degeneracy factor, R_2 is the two-body phase space integral as defined in [33], and s is the center of mass energy squared. It is directly proportional to the $2 \rightarrow 3$ cross section, i.e.,

$$I_{32} = \frac{192\pi^2}{d} \sigma_{23} = 12\pi^2 \sigma_{23}. \quad (3)$$

The inclusion of radiative processes couples the chemical equilibration to the kinetic equilibration. If the system is not far from chemical equilibrium, then the inclusion of radiative processes will lead to additional collisions and isotropization. If the system is far below chemical equilibrium, there will be significant particle production. This will lead to smaller cross sections which will limit the additional isotropization relative to the case with only elastic processes. If the system is far above chemical equilibrium, the decrease in particle number will lead to larger cross sections and enhanced isotropization.

Pressure anisotropy evolutions with elastic collisions only and with radiative processes are compared in Fig. 1. First, let us focus on panel (b) and discuss some of the general features of the evolutions. There are two curves for the case including $2 \leftrightarrow 3$. One is for the case starting with an initial isotropic distribution, i.e., initial $P_L/P_T = 1$. The other is for the case with an inside-outside type of initial distribution, i.e., initial $P_L/P_T = 0$. Even though they start from quite different initial pressure anisotropies, they approach the same asymptotic evolution at late times. In other words, the memory of initial anisotropy is lost after some characteristic time. The case with only $2 \rightarrow 2$ collisions has approximately the same behavior. The two curves approach and meet each other at late times. This feature is the same for all other cases. The importance of radiative processes is reflected in the difference of the radiative case and the case with only elastic collisions. The radiative case has a pressure anisotropy of about 0.78 at 2 fm/c, significantly larger than that of the elastic only case of 0.65. This shows that radiative processes can significantly enhance thermalization.

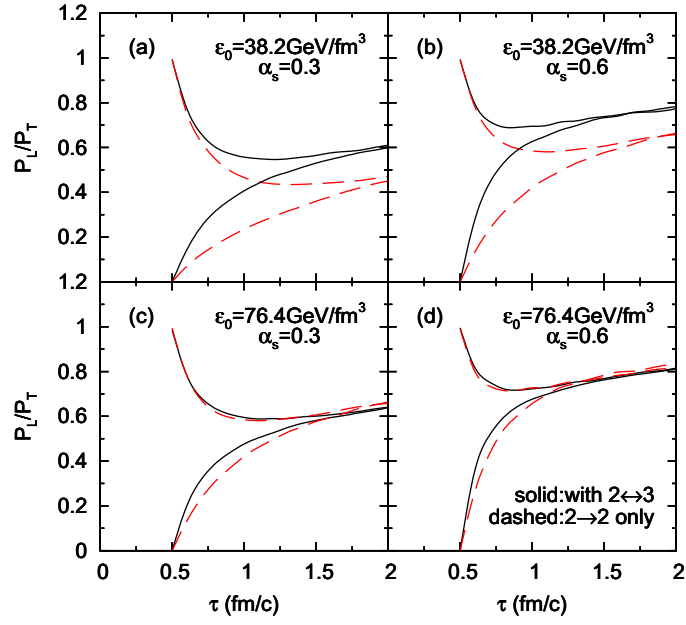


Figure 1: Pressure anisotropy evolution. Solid curves are for the case including the $2 \leftrightarrow 3$ processes while dashed curves are for the case with $2 \rightarrow 2$ only. The upper panels have initial energy density $\epsilon_0 = 38.2 \text{ GeV/fm}^3$ while the lower panels have $\epsilon_0 = 76.4 \text{ GeV/fm}^3$. The left panels are calculated with $\alpha_s = 0.3$ while the right panels have $\alpha_s = 0.6$.

When α_s decreases from 0.6 to 0.3, the asymptotic value at 2 fm/c decreases for both the case with $2 \leftrightarrow 3$ and without $2 \leftrightarrow 3$. When the initial energy density increases from 38.2 GeV/fm³, the case with $2 \leftrightarrow 3$ increases slightly leading to an approximate α_s scaling insensitive to the initial energy density. In contrast, the case with only the $2 \rightarrow 2$ process increases drastically. Because of the slight increase in the radiative case and drastic increase in the elastic only case as the energy density increases, when the initial energy density $\epsilon_0 = 76.4$ GeV/fm³, the radiative and elastic only cases have about the same pressure anisotropy at 2 fm/c. The elastic only case is sensitive to both the initial energy density and the coupling constant. The large initial energy density and small coupling constant case is related to the small initial energy density and large coupling constant case via the $\epsilon_0 \alpha_s$ scaling. The elastic only curves in panel (b) and panel (c) follow this $\epsilon_0 \alpha_s$ scaling and are identical for these two cases.

The above analysis demonstrates that evolutions with and without radiative processes have different dependences on system parameters. In the case with radiative processes, when the energy density is increased, the screening mass decreases, increasing the cross section and collision rate. However, this is counteracted by the additional particle production. As the system falls far below chemical equilibrium, additional particle production tends to increase the screening mass and reduce the collision rate. Lacking this balancing factor, the elastic only case cannot maintain approximately the same evolution as with the lower energy density case and the pressure anisotropy increases drastically. Decreasing the coupling constant can compensate for the increase in pressure anisotropy caused by the energy density increase. As the initial binary collision cross section is proportional to $\epsilon_0 \alpha_s$ with fixed initial number density, when the coupling constant is decreased by the same factor as the energy density increase, there is an exact $\epsilon_0 \alpha_s$ scaling in the elastic only case. This is qualitatively different from the approximate α_s scaling in the radiative case.

The two data sets with different initial pressure anisotropies but otherwise same parameters seem to converge toward a common final evolution. The difference between these two data sets can be used to study the rate of convergence as shown in Fig. 2 for cases including the $2 \leftrightarrow 3$ processes. The difference quickly decreases and at late times fits well with an exponential decrease with proper time. In the case with $2 \rightarrow 2$ only, the two curves may cross each other at late times (see e.g. panel (d) in Fig. 1). In any case, by 2 fm/c, the differences all go to about or below 1% of the initial difference.

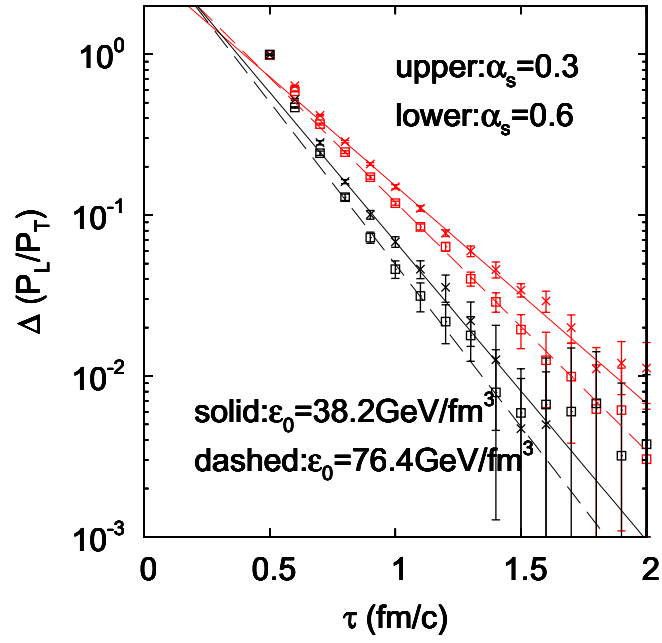


Figure 2: Pressure anisotropy difference evolution. These results all include the radiative processes. Crosses (squares) are for initial energy density $\epsilon_0 = 38.2(76.4)$ GeV/fm^3 . Solid and dashed curves are exponential fits for $\tau \geq 0.8$ fm/c . For the two data sets with the same symbol, the upper one is for $\alpha_s = 0.3$ and the lower one is for $\alpha_s = 0.6$.

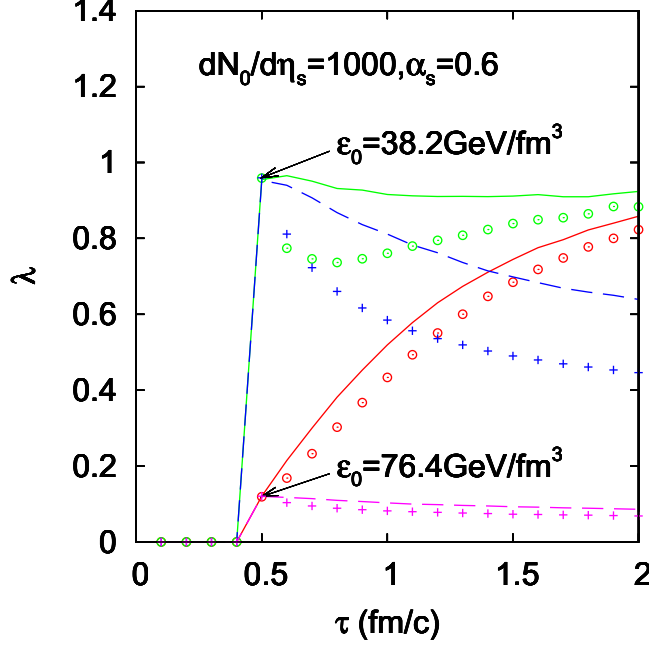


Figure 3: Proper time evolution of fugacity λ for initial space-time rapidity density $dN_0/d\eta_s = 1000$ and coupling constant $\alpha_s = 0.6$. Lines are for isotropic exponential initial conditions and points are for transverse exponential initial conditions. Solid lines and circles are results including $2 \leftrightarrow 3$. Dashed lines and pluses are results with $2 \rightarrow 2$ only. For the two data sets with the same symbol, the upper one is for $\epsilon_0 = 38.2 \text{ GeV/fm}^3$ and the lower one is for $\epsilon_0 = 76.4 \text{ GeV/fm}^3$.

The system approaches the asymptotic evolution on a very short time scale. The comparison in Fig. 2 shows that the approach to asymptotic evolution is faster with higher initial energy density or higher coupling constant. It is interesting to notice that within error bars, these lines seem to go through the same point. We also looked at the curves with only elastic processes. They also seem to go through a common point, even though that point is different from the one with inelastic processes.

To get a better understanding of the relation between the observed pressure isotropization and radiative processes, it is helpful to look at the fugacity evolution. Define fugacity to be the ratio of particle density to the equilibrium particle density, i.e., $\lambda = n/n_{eq}$. When the temperature T is taken to be the average kinetic energy per degree of freedom, i.e., $T = \epsilon/(3n)$, the resultant n_{eq} leads to the expression $\lambda = 27\pi^2 n^4/(16\epsilon^3)$. For systems

in thermodynamical equilibrium, i.e., in chemical and thermal equilibrium, $\lambda = 1$. The comparison of fugacity evolutions in Fig. 3 demonstrates the interplay between thermal equilibration and chemical equilibration. Transverse initial conditions have evolutions lower than their isotropic initial condition counterparts mainly because of their slower early energy density evolutions caused by the inside-outside space-momentum correlation. When only $2 \rightarrow 2$ is included, the system falls farther and farther away from chemical equilibrium. As the $2 \leftrightarrow 3$ processes are turned on, the system is able to approach chemical equilibrium. Even for transverse initial conditions with $\epsilon_0 = 38.2$ GeV/fm³ where there is a decrease in fugacity mainly due to longitudinal expansion, at late times, the fugacity is able to reach a value that is comparable to other cases. Note that in this case, there are more annihilations than productions initially even when $\lambda \sim 1$ because of the transverse spatial distribution. This is why the early evolution is slightly lower than the corresponding elastic only case. It demonstrates that chemical equilibration depends on kinetic equilibration in the radiative case. For various cases with the $2 \leftrightarrow 3$ processes, the final fugacities at 2 fm/c are all on the 80% to 90% level. Note that the $\epsilon_0 = 38.2$ GeV/fm³ case has an initial fugacity close to 1, while the $\epsilon_0 = 76.4$ GeV/fm³ case is significantly undersaturated initially. As discussed before, this difference in initial fugacities is behind the observed different energy dependences of pressure anisotropy evolutions for the elastic only and the radiative cases.

3. Summary and discussions

The above study demonstrates the different behaviors of evolutions with and without radiative processes. When radiative processes are included, there is an approximate α_s scaling that is in contrast with the $\epsilon_0 \alpha_s$ scaling seen when only elastic processes are included. Evolutions with different initial pressure anisotropies appear to approach the same asymptotic evolution exponentially at late times. If a partonic system is initially close to chemical equilibrium, radiative processes can significantly enhance pressure isotropization. For systems significantly undersaturated at the initial time, evolutions with and without radiative processes can be close to each other. This dependence on initial fugacity indicates that it may be necessary to use different K factors for elastic simulations at different collision energies.

The above calculations start with initial exponential momentum distributions. The dependence on the initial momentum distribution can be studied

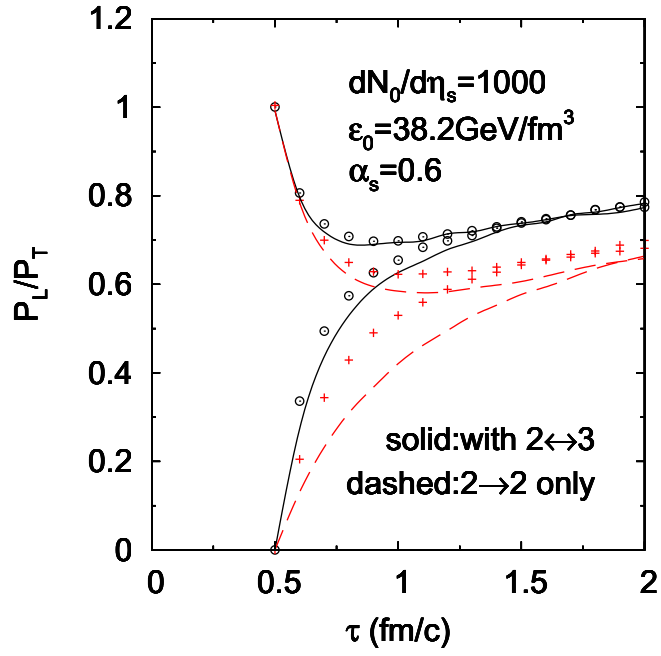


Figure 4: Pressure anisotropy evolution for $dN_0/d\eta_s = 1000$, $\epsilon_0 = 38.2 \text{ GeV/fm}^3$, $\alpha_s = 0.6$. Lines are for exponential initial momentum distributions and points are for condensate initial momentum distributions. Solid lines and circles are for the case including the $2 \leftrightarrow 3$ processes while dashed lines and pluses are for the case with $2 \rightarrow 2$ only.

by comparing the results with those that start with initial momentum distributions motivated by the Color Glass Condensate. Fig. 4 has additional calculations with step function initial momentum distributions. A clear enhancement of pressure isotropization is observed with the step function initial distributions when only elastic processes are included. When inelastic processes are included, there is not much change in the pressure anisotropy evolution. In other words, the pressure isotropization is robust against changes in the initial momentum distribution. This difference between the elastic only and with radiative reflects the faster thermalization when radiative processes are included. Without them, the step function momentum distribution maintains its shape for a longer period of time, resulting in a smaller screening mass and larger collision rate per particle and a significant change in the pressure anisotropy evolution. This comparison demonstrates again the importance of radiative processes in microscopic simulations of relativistic heavy ion collisions.

Acknowledgments

We thank S. Bass, R. Bellwied, F. Gelis, H. Grigoryan, M. Guenther, U. Heinz, S. Katz, V. Koch, M. Lisa, L. McLerran, H. Meyer, U. Mosel, S. Pratt, I. Vitev, H. Zhou for helpful discussions and the Parallel Distributed Systems Facilities of the National Energy Research Scientific Computing Center for providing computing resources. This work was supported by the U.S. National Science Foundation under grant No.'s PHY-0554930 and PHY-0970104.

References

- [1] I. Arsene, et al., [BRAHMS Collaboration], Nucl. Phys. A **757** (2005) 1 [arXiv:nucl-ex/0410020].
- [2] B. B. Back, et al., [PHOBOS Collaboration], Nucl. Phys. A **757** (2005) 28 [arXiv:nucl-ex/0410022].
- [3] J. Adams, et al., [STAR Collaboration], Nucl. Phys. A **757** (2005) 102 [arXiv:nucl-ex/0501009].
- [4] K. Adcox, et al., [PHENIX Collaboration], Nucl. Phys. A **757** (2005) 184 [arXiv:nucl-ex/0410003].

- [5] D. Teaney, J. Lauret, E. V. Shuryak, Phys. Rev. Lett. **86** (2001) 4783 [arXiv:nucl-th/0011058].
- [6] P. Huovinen, P. F. Kolb, U. W. Heinz, P. V. Ruuskanen, S. A. Voloshin, Phys. Lett. B **503** (2001) 58 [arXiv:hep-ph/0101136].
- [7] P. F. Kolb, U. W. Heinz, P. Huovinen, K. J. Eskola, K. Tuominen, Nucl. Phys. A **696** (2001) 197 [arXiv:hep-ph/0103234].
- [8] T. Hirano, U. W. Heinz, D. Kharzeev, R. Lacey, Y. Nara, Phys. Lett. B **636** (2006) 299 [arXiv:nucl-th/0511046].
- [9] S. A. Bass, B. Müller, D. K. Srivastava, Phys. Lett. B **551** (2003) 277 [arXiv:nucl-th/0207042].
- [10] D. Molnár, M. Gyulassy, Nucl. Phys. A **697** (2002) 495, Nucl. Phys. A **703** (2002) 893(E) [arXiv:nucl-th/0104073].
- [11] B. Zhang, C. M. Ko, B. A. Li, Z. W. Lin, Phys. Rev. C **61** (2000) 067901 [arXiv:nucl-th/9907017].
- [12] Z. W. Lin, S. Pal, C. M. Ko, B. A. Li, B. Zhang, Phys. Rev. C **64** (2001) 011902 [arXiv:nucl-th/0011059].
- [13] Z. W. Lin, S. Pal, C. M. Ko, B. A. Li, B. Zhang, Nucl. Phys. A **698** (2002) 375 [arXiv:nucl-th/0105044].
- [14] Z. W. Lin, C. M. Ko, B. A. Li, B. Zhang, S. Pal, Phys. Rev. C **72** (2005) 064901 [arXiv:nucl-th/0411110].
- [15] Z. Xu, C. Greiner, Phys. Rev. C **71** (2005) 064901 [arXiv:hep-ph/0406278].
- [16] G. Ferini, M. Colonna, M. Di Toro, V. Greco, Phys. Lett. B **670** (2009) 325 [arXiv:0805.4814 [nucl-th]].
- [17] U. W. Heinz, arXiv:0901.4355 [nucl-th].
- [18] A. Muronga, Phys. Rev. Lett. **88** (2002) 062302 [Erratum-ibid. **89** (2002) 159901] [arXiv:nucl-th/0104064].
- [19] K. Dusling, D. Teaney, Phys. Rev. C **77** (2008) 034905 [arXiv:0710.5932 [nucl-th]].

- [20] M. Luzum, P. Romatschke, Phys. Rev. C **78** (2008) 034915 [arXiv:0804.4015 [nucl-th]].
- [21] H. Song, U. W. Heinz, Phys. Rev. C **77** (2008) 064901 [arXiv:0712.3715 [nucl-th]].
- [22] H. Song, U. W. Heinz, Phys. Rev. C **78** (2008) 024902 [arXiv:0805.1756 [nucl-th]].
- [23] H. Song, U. W. Heinz, Phys. Lett. B **658** (2008) 279 [arXiv:0709.0742 [nucl-th]].
- [24] G. S. Denicol, T. Koide, D. H. Rischke, arXiv:1004.5013 [nucl-th].
- [25] J. Berges, S. Borsanyi, C. Wetterich, Nucl. Phys. B **727** (2005) 244 [arXiv:hep-ph/0505182].
- [26] W. Florkowski, Phys. Lett. B **668** (2008) 32 [arXiv:0806.2268 [nucl-th]].
- [27] P. M. Chesler, L. G. Yaffe, Phys. Rev. Lett. **102** (2009) 211601 [arXiv:0812.2053 [hep-th]].
- [28] P. M. Chesler, L. G. Yaffe, Phys. Rev. D **82** (2010) 026006 [arXiv:0906.4426 [hep-th]].
- [29] Z. Xu, C. Greiner, Phys. Rev. C **76** (2007) 024911 [arXiv:hep-ph/0703233].
- [30] B. Zhang, L. W. Chen, C. M. Ko, J. Phys. G **35** (2008) 065103 [arXiv:0705.3968 [nucl-th]].
- [31] P. Huovinen, D. Molnar, Phys. Rev. C **79** (2009) 014906 [arXiv:0808.0953 [nucl-th]].
- [32] A. El, Z. Xu, C. Greiner, Phys. Rev. C **81** (2010) 041901 [arXiv:0907.4500 [hep-ph]].
- [33] R. Hagedorn, Relativistic Kinematics, W.A. Benjamin Inc., New York, 1964.